# Chapter 8

# Results and Conclusions

First, a brief discussion of the convolution of a Breit-Wigner resonance with the beam energy distribution is presented. The method of determining resonance parameters is presented before the results of the analyses are presented. In conclusion, the significance of the signals is discussed and upper limits of the products of branching ratios are presented.

## 8.1 Expected Cross Sections

The Breit-Wigner cross section, as a function of center of mass energy $E_{cm}$, for the formation by $\bar{p}p$ annihilation and decay of a resonance $R$ of spin $J$, mass $M_R$ and total width $\Gamma_R$ is

$$\sigma_{BW}(E_{cm}) = \frac{(2J+1)}{(2S_p+1)(2S_{\bar{p}}+1)} \frac{4\pi(\hbar c)^2}{(E_{cm}^2 - 4(m_p c^2)^2)} \frac{\Gamma_R^2 B_{in} B_{out}}{(E_{cm} - M_R c^2)^2 + \Gamma_R^2/4}, \quad (8.1)$$

where $S_i$ is spin for the proton and antiproton, $B_{in}$ and $B_{out}$ are the branching ratios for the resonance's formation channel ($\bar{p}p \to R$) and decay channel, respectively. The decay branching ratio contains all subsequent decays to the final state particles.

When $E_{cm} = M_R c^2$, the cross section for a particular final state becomes

$$\sigma_{peak} = \frac{(2J+1)4\pi\hbar^2 B_{in} B_{out}}{(M_R^2 - 4m_p^2)c^2}. \tag{8.2}$$

When the resonance is the $^1\mathrm{P}_1$ and the mass is taken to be near $M_{\chi_{cog}}$, the peak cross section becomes

$$\sigma_{peak} = 1.64 \text{ mb} \times B(^1\mathrm{P}_1 \to \bar{p}p) \times B(^1\mathrm{P}_1\ decay) \times B(subsequent\ decays); \tag{8.3}$$

of course, the measured peak cross section is further reduced by the total efficiency.

The beam energy width is finite, which results in the cross section for any point being the convolution of a Breit-Wigner resonance with the center of mass energy distribution:

$$\sigma(E_{cm}) = \int_0^\infty \sigma_{BW}(E') F_{beam}(E' - E_{cm}) dE', \tag{8.4}$$

where $F_{beam}$ is the center of mass energy distribution due to the beam spread. The beam spread is determined from the spread in revolution frequencies, equation 2.3. In the center of mass frame, the energy is related to the frequency by (equation 7.46)

$$E_{cm}^2 = 2m_p^2 c^4 \left(1 + \frac{1}{\sqrt{1 - (fL/c)^2}}\right). \tag{8.5}$$

The frequency spread, figure 2.5, is used to determine $F_{beam}$; the Schottky noise spectrum is approximated by a gaussian. For determining a run's beam energy distribution, the Schottky noise spectra associated with the run are averaged to get the beam frequency distribution.

## 8.2 Method of Fitting Data

A datum point for fitting consists of events grouped according to runs, energy bins, or stacks. When grouped by runs, the datum point's energy and integrated luminosity are the run's energy and integrated luminosity. If energy bins or stacks are used to group the events, the datum point's energy is calculated by the integrated luminosity weighted average of the energies of the runs.

Data points are then fitted by using a maximum likelihood method. The expected number of events for a datum point $\nu_i$ is a function of the cross section (equation 8.4), the total integrated luminosity $\mathcal{L}_i$, the total efficiency $\epsilon_{tot}$ associated with the point, and a background cross section $\sigma_{bkg}$:

$$\nu_i = \mathcal{L}_i \times [\sigma(E_{cm,i}) \times \epsilon_{tot} + \sigma_{bkg}]. \tag{8.6}$$

The likelihood function $\Lambda$ for $N$ data points is the product of $N$ Poisson functions,

$$\Lambda = \prod_{i=1}^{N} \frac{\nu_i^{n_i} e^{-\nu_i}}{n_i!}, \tag{8.7}$$

where $n_i$ is the number of events observed for the $i^{th}$ datum point. The log-likelihood function, $\ln(\Lambda)$, is maximized resulting in fitted values for the mass, width, product of branching ratios $(B_{in}B_{out})$, and the background cross section.

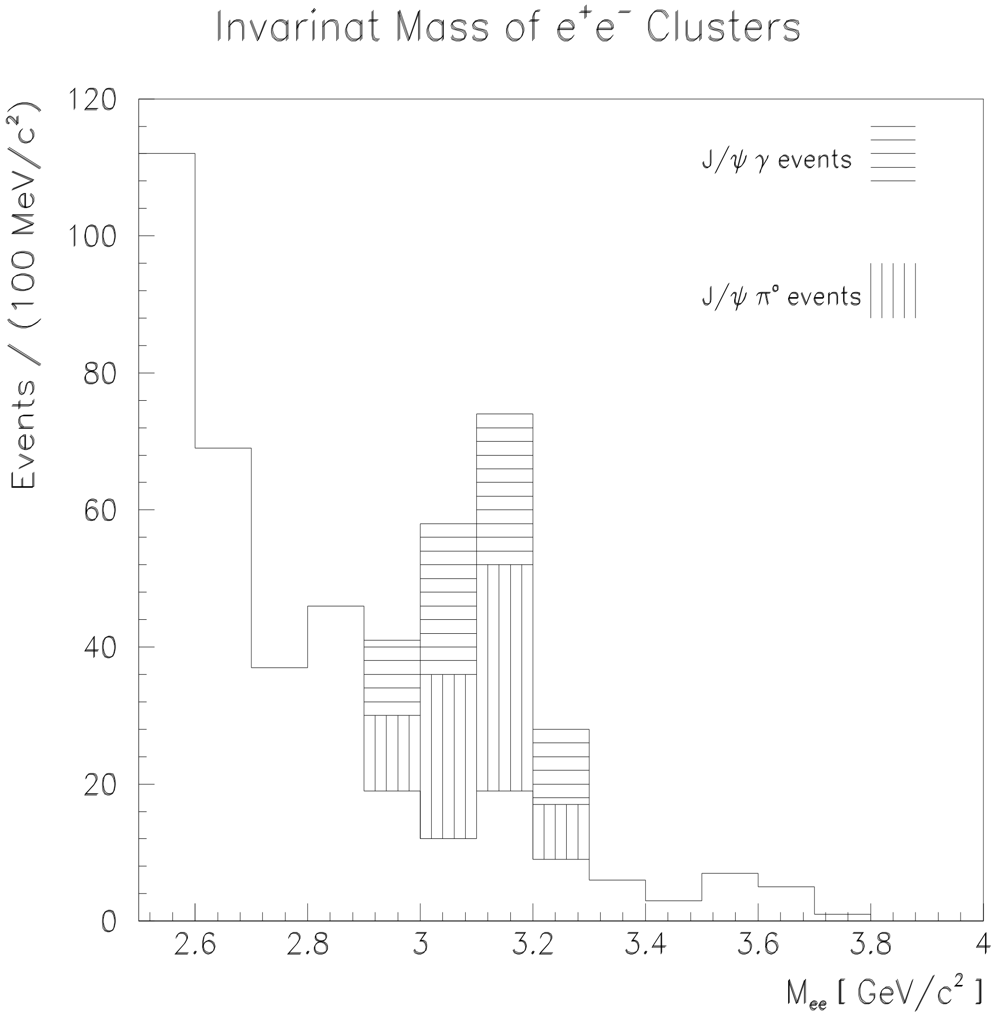


Figure 8.1: The reconstructed invariant mass of the $e^+e^-$ pair for all 16 stacks.

## 8.3 Charged Channels

The reconstructed invariant masses of the two tracks associated with the $e^+e^-$ pair, are shown in figure 8.1; events from all 16 stacks are shown. The excess of events at 3.1 GeV/c$^2$ are inclusive $J/\psi$ events. These events are identified as either $J/\psi\pi^o$ or $J/\psi\gamma$; the number of events of each type is shown in table 8.1. The possible reasons for the $J/\psi\gamma$ events is presented after the results of fitting the $J/\psi\pi^o$ data set.

| Stack | $J/\psi\pi^o$ | $J/\psi\gamma$ | Stack | $J/\psi\pi^o$ | $J/\psi\gamma$ |
|---|---|---|---|---|---|
| 1 | 1 | 4 | 9 | 4 | 7 |
| 2 | 2 | 4 | 10 | 8 | 6 |
| 3 | 3 | 4 | 11 | 3 | 3 |
| 4 | 1 | 4 | 12 | 9 | 4 |
| 5 | 2 | 8 | 13 | 6 | 4 |
| 6 | 10 | 3 | 14 | 7 | 3 |
| 7 | 3 | 4 | 15 | 4 | 2 |
| 8 | 8 | 8 | 16 | 3 | 1 |

Table 8.1: The number of $J/\psi\pi^o$ and $J/\psi\gamma$ events for each stack.

### 8.3.1 $J/\psi\pi^o$ Events

The number of events divided by the integrated luminosity for each stack is shown in figure 8.2. In figure 8.3, the events from runs with center of mass energies near 3526 MeV are grouped into 200 keV bins. In both figures, there appears to be a larger observed cross section around 3526 MeV with a 2 pb background.

The events grouped by stack or by bins of 100, 200 and 300 keV, have been subjected to the maximum likelihood analysis described in the previous section. In each case, the resonance width has had to be fixed; if left to vary, the result is zero width due to the small statistics and large beam width. The resonance width is fixed at values from 250 keV up to 1250 keV in increments of 250 keV. The mass is found to be $3526.15 \pm 0.15$ MeV/c$^2$ (statistical error from the fit); the other parameters are dependent upon the fixed resonance width and are presented in table 8.2. An upper limit (90% $CL$) of 1.1 MeV for the resonance width is set. If the data for all sixteen stacks are fit to a flat background, the cross section is 4.7 events per pb$^{-1}$.

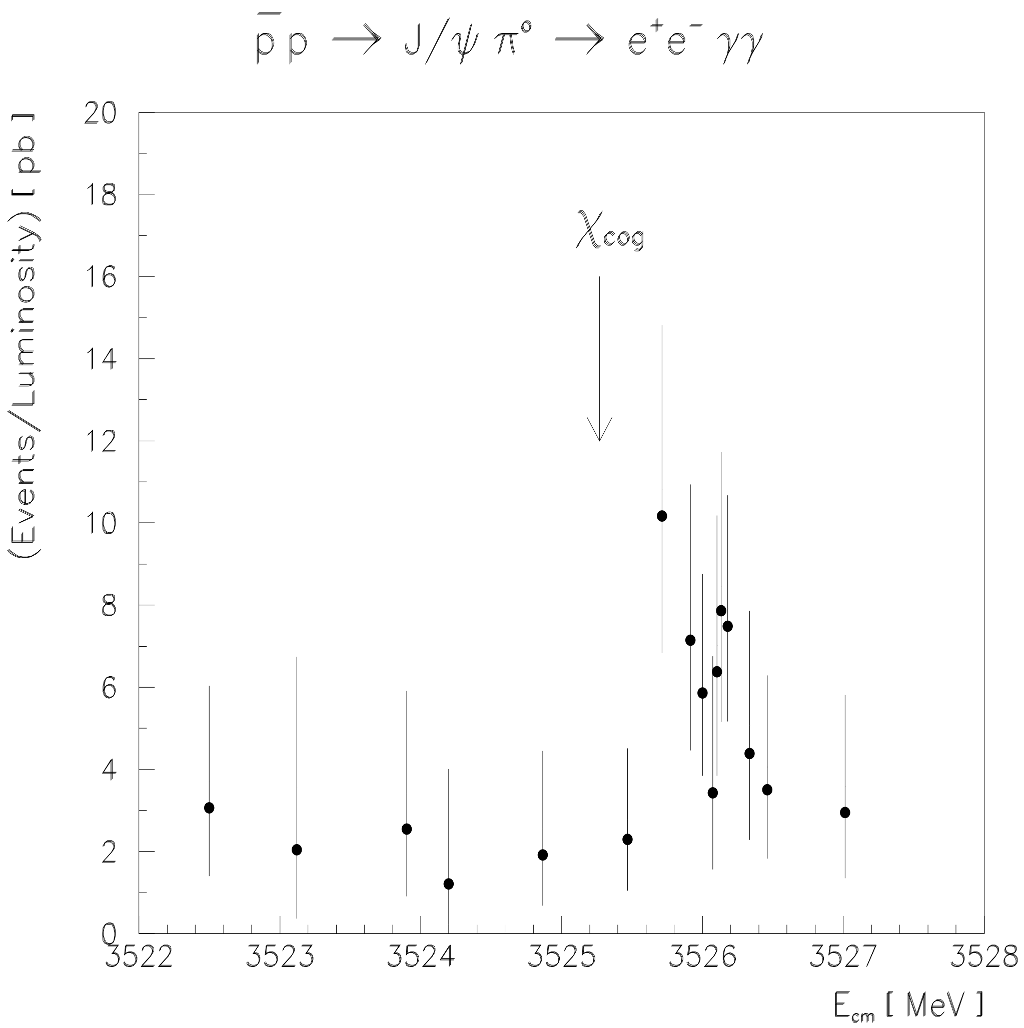


Figure 8.2: The number of events divided by integrated luminosity for each stack. The error bars are statistical.

The ratio of the maximum values of the likelihood functions for the hypothesis of a resonance and a background, $\Lambda(H_1)$, to the flat background hypothesis, $\Lambda(H_0)$, is used to form a test statistic $\xi = -2\ln\lambda$ where $\lambda = \Lambda(H_0)/\Lambda(H_1)$ [80]. The probability that a fictitious resonance results from fluctuations of a flat background has been investigated with Monte Carlo simulations of the data points; E760 data points' energies and integrated luminosities are used along with Possion distributed numbers of events based upon the fit to a flat cross section, 4.7 events per $\mathrm{pb}^{-1}$. The

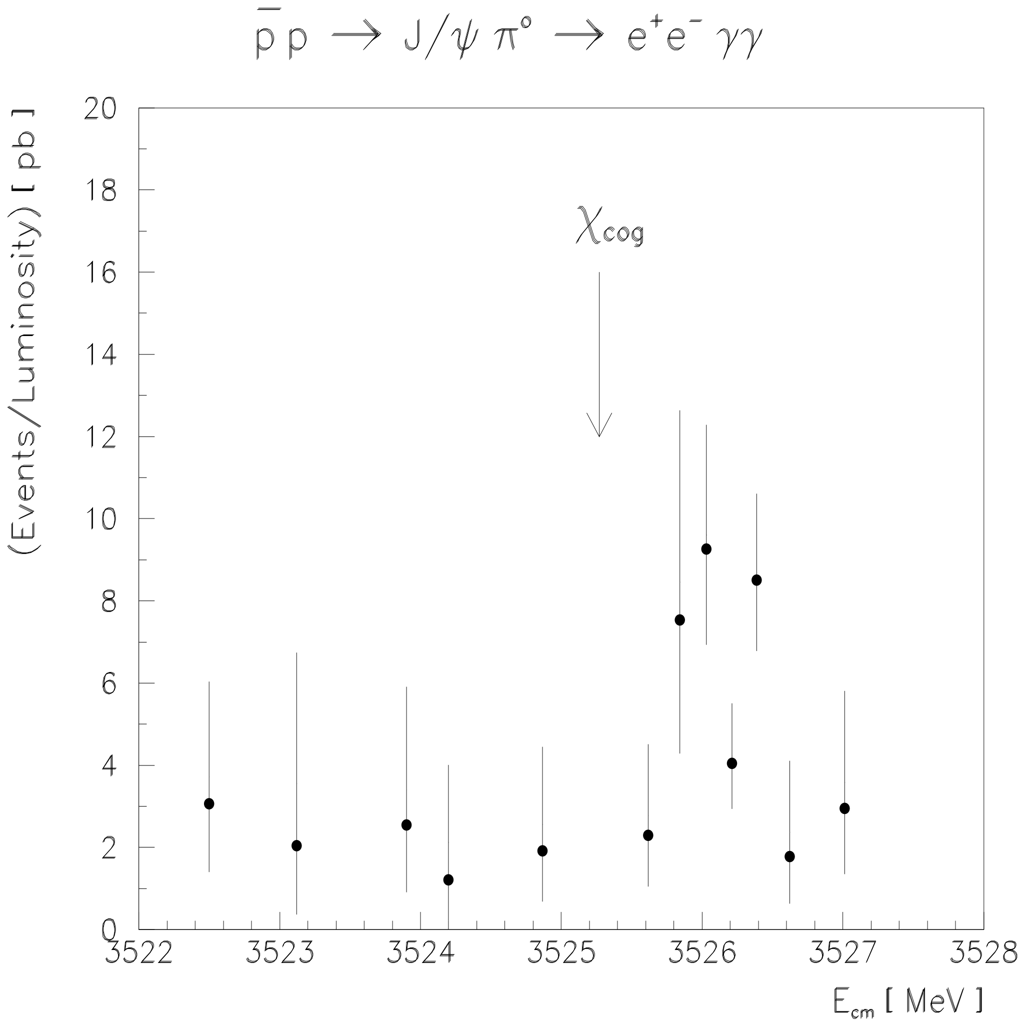


Figure 8.3: Same as figure 8.2 except for runs near 3526 MeV/c$^2$ are grouped in 200 keV bins. The error bars are statistical.

Monte Carlo experiments are fitted in the same manner as above and the test statistic is calculated; the percentage of the Monte Carlo test statistics $\xi_{MC}$ which are greater than the real experiment's test statistic $\xi_{exp}$ gives the statistical significance of the resonance. Table 8.3 shows $\xi_{exp}$ and the statistical significance based upon 10,000 Monte Carlo experiments for different energy bin widths and resonance widths.

| Width (keV) | $B(^1\mathrm{P}_1 \to \bar{p}p) \times B(^1\mathrm{P}_1 \to J/\psi\pi^o)$ ($\times 10^{-7}$) | $\sigma_{bkg}$ (pb) |
|---|---|---|
| 250 | 1.0 $\pm$ 0.3 | 2.1 $\pm$ 0.3 |
| 500 | 1.2 $\pm$ 0.4 | 1.9 $\pm$ 0.2 |
| 750 | 1.5 $\pm$ 0.4 | 1.8 $\pm$ 0.2 |
| 1000 | 1.7 $\pm$ 0.5 | 1.7 $\pm$ 0.2 |
| 1250 | 2.0 $\pm$ 0.5 | 1.6 $\pm$ 0.2 |

Table 8.2: The resulting values of the fit parameters for fixed resonance widths. The resonance mass is independent of the resonance width and is found to be 3526.15 $\pm$ 0.15 MeV/c$^2$ (this error and the table's entry errors are statistical and from the fit).

| Bin Width (keV) | $\Gamma_R$ (keV) | $\xi_{exp}$ | Statistical Significance |
|---|---|---|---|
| 100 | 250 | 14.0 | 0.6 $\times 10^{-3}$ |
| 100 | 500 | 13.3 | 1.5 $\times 10^{-3}$ |
| 100 | 750 | 12.6 | 1.7 $\times 10^{-3}$ |
| 100 | 1000 | 11.9 | 2.5 $\times 10^{-3}$ |
| 100 | 1250 | 11.2 | 3.1 $\times 10^{-3}$ |
| 200 | 250 | 13.9 | 0.6 $\times 10^{-3}$ |
| 200 | 500 | 13.3 | 0.7 $\times 10^{-3}$ |
| 200 | 750 | 12.6 | 1.2 $\times 10^{-3}$ |
| 200 | 1000 | 12.0 | 1.9 $\times 10^{-3}$ |
| 200 | 1250 | 11.3 | 2.6 $\times 10^{-3}$ |
| 300 | 250 | 13.2 | 1.3 $\times 10^{-3}$ |
| 300 | 500 | 12.7 | 1.9 $\times 10^{-3}$ |
| 300 | 750 | 12.1 | 2.4 $\times 10^{-3}$ |
| 300 | 1000 | 11.5 | 3.6 $\times 10^{-3}$ |
| 300 | 1250 | 10.9 | 4.6 $\times 10^{-3}$ |

Table 8.3: The experiment's test statistic $\xi_{exp}$ and the fraction of Monte Carlo experiments with $\xi_{MC} \geq \xi_{exp}$ out of 10,000 simulations, which results in the statistical significance (for different binning of the data and resonance widths).

The 2 events per $\mathrm{pb}^{-1}$ background observed near the resonance corresponds to a continuum cross section $\sigma(\bar{p}p \rightarrow J/\psi\pi^o) \approx 100$ pb, which is in agreement with what is predicted for the continuum [81]. The continuum $J/\psi\pi^o$ cross section is predicted to increase with energy; agreement with this prediction is seen in data taken near $\sqrt{s} \approx 3.6$ GeV, where the continuum cross section is measured to be $\approx 155$ pb.

### 8.3.2 $J/\psi\gamma$ Events

The ${}^1\mathrm{P}_1$ is forbidden to decay radiatively to $J/\psi$ by charge conjugation invariance. The number of $J/\psi\gamma$ events found divided by the integrated luminosity is constant, $\approx$ 4 pb, within the region investigated as shown in figure 8.4. No resonance is evident. The test statistic from fitting the $J/\psi\gamma$ data to a resonance[1] with a flat background is compared to Monte Carlo experiments' test statistics (Poisson distributed number of events based upon a flat cross section); 30% of the Monte Carlo test statistics are larger than the $J/\psi\gamma$ data test statistic, i.e. there is no statistical significance for a $J/\psi\gamma$ resonance.

There are several possible explanations for the $J/\psi\gamma$ events. One possible explanation is that some of these events are actually $J/\psi\pi^o$ events where one of the gamma rays escapes detection, *feed down*; only a few of the events fit this hypothesis. However, at $\sqrt{s} \approx 3.6$ GeV there are a few $J/\psi\gamma$ events which is consistent with feed down from the $J/\psi\pi^o$ continuum.

[1] Fixed widths have been used: between 250 and 1250 keV.

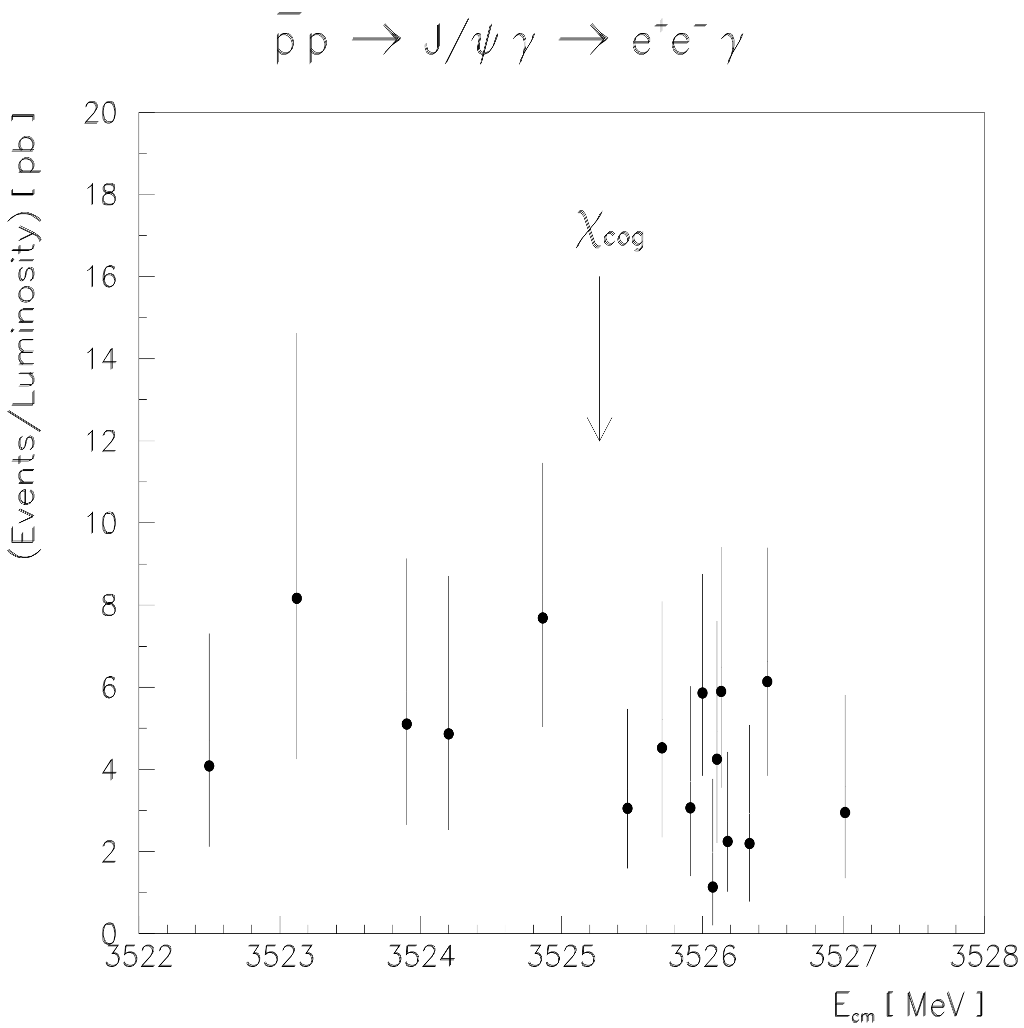


Figure 8.4: The number of events divided by integrated luminosity for each stack. The error bars are statistical.

Using the Breit-Wigner resonance cross section[2] (equation 8.1) for the $\chi_1$ and $\chi_2$ states, cross sections of 2.3 pb and 2.6 pb result, respectively, from the tails of the two triplet P wave resonances. A total efficiency [20] of $\approx 0.4$ for $J/\psi\gamma$ events reduces this to an expected observed cross section of $\approx 2$ pb (the beam energy convolution has not been considered).

[2]The Breit-Wigner resonance shape may not be appropriate for the tails of a resonance.

Another possible explanation involves $\bar{p}$'s that have been straggled by the gas jet. The $\bar{p}$'s lose enough energy so that they are no longer caught in the main frequency harmonic being used for stochastic cooling; however, the new revolution frequencies are stochastically cooled at a different harmonic, and therefore the lower energy $\bar{p}$'s stay in the machine. Unfortunately, there is no measurement of this phenomenon; the momentum pickup's Schottky noise spectrum shows a long lowside tail (as in figure 2.5) and eventually a second peak (not pictured) which has only been observed and not recorded. It is possible that such a second peak at lower energy, convoluted with the $\chi_1$ resonance, results in a $J/\psi\gamma$ cross section consistent with that observed.

### 8.3.3 $J/\psi\pi\pi$ Results

No events fit exclusively either of the $J/\psi\pi\pi$ channels. The 90% $CL$ upper limits for the product of branching ratios are

$$B(^1\mathrm{P}_1 \to \bar{p}p) \times B(^1\mathrm{P}_1 \to J/\psi\pi^o\pi^o) \quad \leq 2.1 \times 10^{-8}, \tag{8.8}$$

$$B(^1\mathrm{P}_1 \to \bar{p}p) \times B(^1\mathrm{P}_1 \to J/\psi\pi^+\pi^-) \quad \leq 4.3 \times 10^{-8}. \tag{8.9}$$

## 8.4 Neutral Channels

The $3\gamma$ channel shows no evidence for a resonance as seen in figure 8.5. The data can be used to set an upper limit on the product of branching ratios. The same

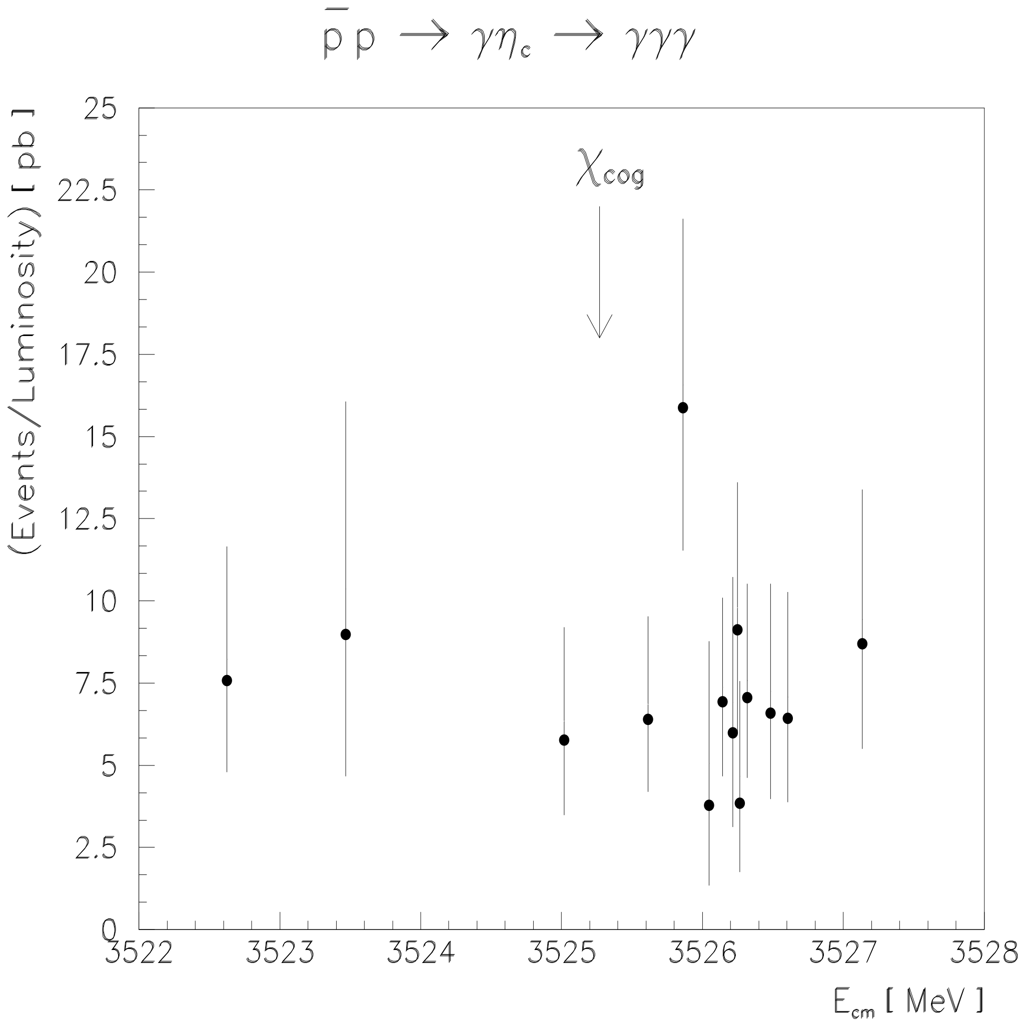


Figure 8.5: The results of the search for $\eta_c\gamma \rightarrow 3\gamma$ final state.

method will be used to set upper limits for the product of branching ratios for the $7\gamma$ final states.

An upper limit is placed by comparing the data from stacks which are in the resonance region with the data from outside of the peak region; the resonance region is defined to be $\pm 400$ keV/c$^2$ of the $^1P_1$ mass as found by the $J/\psi\pi^o$ analysis. The number of events in the resonance region, $n_R$, is assumed to have two contributions, the resonance ($N_R$) and the background ($N_B$); the number of events attributed to the background is determined from the non-resonance region number of events $n_B$:

$$N_B = n_B \times \frac{\mathcal{L}_{peak}}{\mathcal{L}_{off}}, \tag{8.10}$$

where $\mathcal{L}_{peak}$ and $\mathcal{L}_{off}$ are the sums of the integrated luminosities of the stacks in the resonance and non-resonance regions, respectively. The number of events attributed to the resonance is

$$N_R = n_R - N_B; \tag{8.11}$$

assuming Poisson statistics, the uncertainty is

$$\Delta N_R = \sqrt{n_R + n_B \times \left(\frac{\mathcal{L}_{peak}}{\mathcal{L}_{off}}\right)^2}. \tag{8.12}$$

The 90% $CL$ upper limit for the number of resonance events $N_L$ is determined when the integral of a gaussian (mean $N_R$, $\sigma = \Delta N_R$, and integration limits of 0 and $N_L$) is equal to 0.9 of the integral from 0 to $\infty$. The corresponding product of branching ratios upper limit for the resonance region is found using the equation for the peak cross section (equation 8.3) and the total efficiency.

For the $3\gamma$ final state, the number of extra events in the resonance region[3] is 3.6 with an uncertainty of 10.8; the 90% $CL$ upper limit to the number of events is 20.6 events (which corresponds to an efficiency corrected cross section of 19.6 pb, the final efficiency can be found in table 7.11). Using $B(\eta_c \to \gamma\gamma) = 3.47 \times 10^{-4}$ [82], the 90% $CL$ upper limit is

$$B(^1\mathrm{P}_1 \to \bar{p}p) \times B(^1\mathrm{P}_1 \to \gamma\eta_c) \leq 3.44 \times 10^{-5}. \tag{8.13}$$

[3]When this is done for the $J/\psi\pi^o$ data, the number of events attributed to the resonace is 34.2 and the uncertainty is 8.8; in contrast, for the $J/\psi\gamma$ data the excess number of events is $-6.3$ with an uncertainty of 8.5.

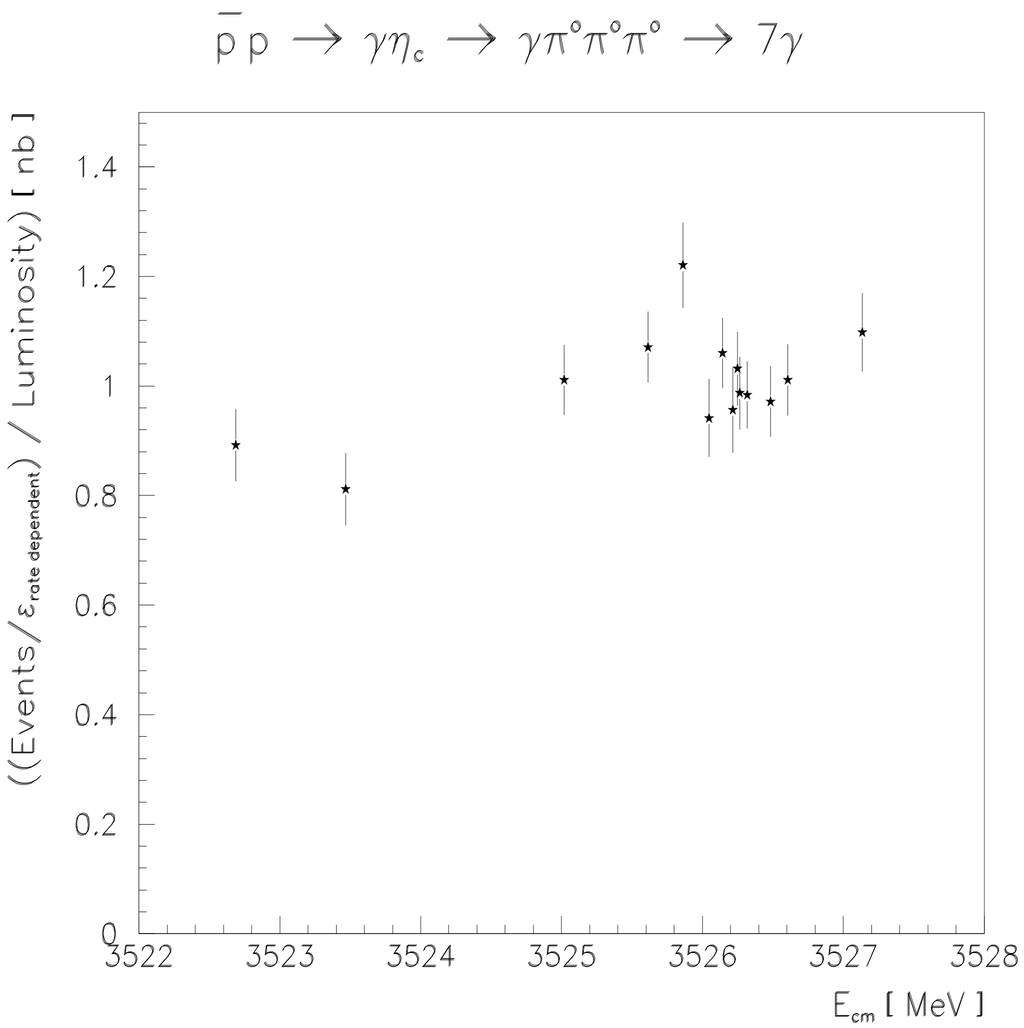


Figure 8.6: The results of the search for a resonance from $\bar{p}p \rightarrow \eta_c\gamma \rightarrow \pi^o\pi^o\pi^o\gamma$, a $7\gamma$ final state. The number of events is corrected on a run by run basis for the rate dependent efficiencies (binned by stack).

The number of events for a stack, corrected on a run by run basis for the rate dependent efficiencies, divided by the integrated luminosity for the stack is shown for the $7\gamma$ final states in figures 8.6 to 8.18. Each datum point of the plots is the sum for a stack of the rate dependent corrected values of the numbers of events for the runs ($N_{run}$),

$$\sum_{run} \frac{N_{run}}{\frac{\epsilon_{H1}}{\alpha_{pu}} \times \epsilon_{FCAL} \times \epsilon_{ETOT-hard} \times \epsilon_{ETOT-soft} \times \epsilon_{ecc} \times \epsilon'_{ecf}}, \tag{8.14}$$

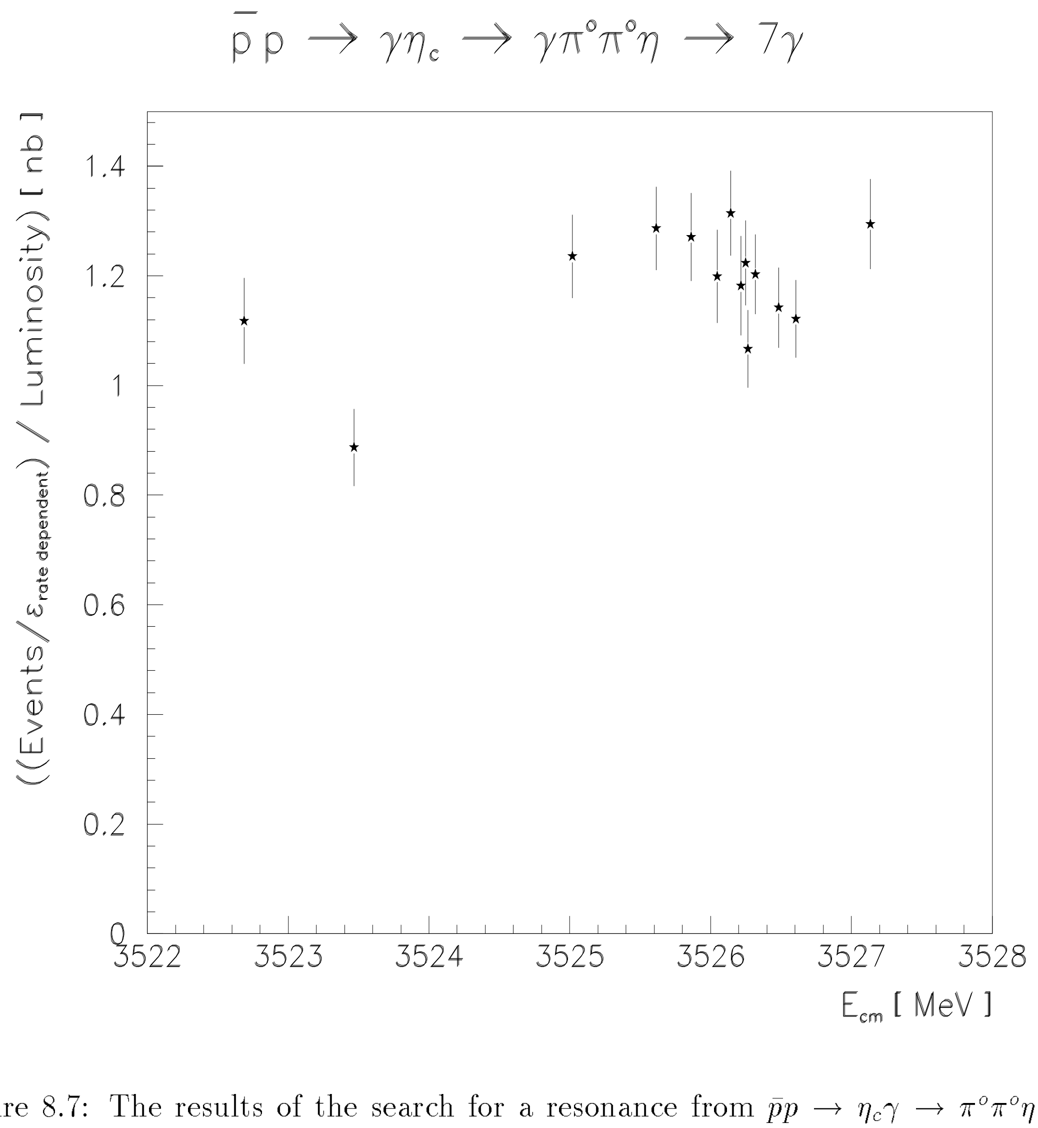


Figure 8.7: The results of the search for a resonance from $\bar{p}p \rightarrow \eta_c\gamma \rightarrow \pi^o\pi^o\eta\gamma$, a $7\gamma$ final state. The number of events is corrected on a run by run basis for the rate dependent efficiencies (binned by stack).

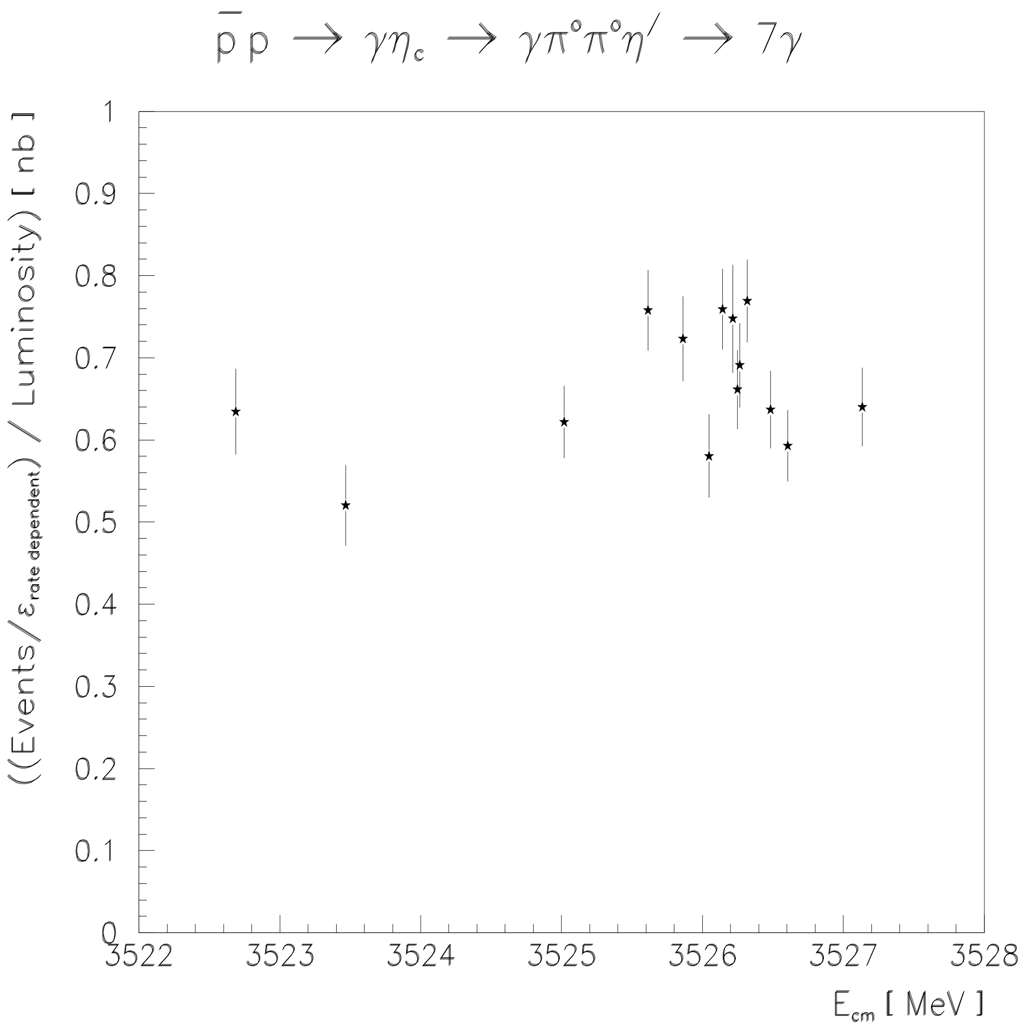


Figure 8.8: The results of the search for a resonance from $\bar{p}p \rightarrow \eta_c\gamma \rightarrow \pi^o\pi^o\eta'\gamma$, a $7\gamma$ final state. The number of events is corrected on a run by run basis for the rate dependent efficiencies (binned by stack).

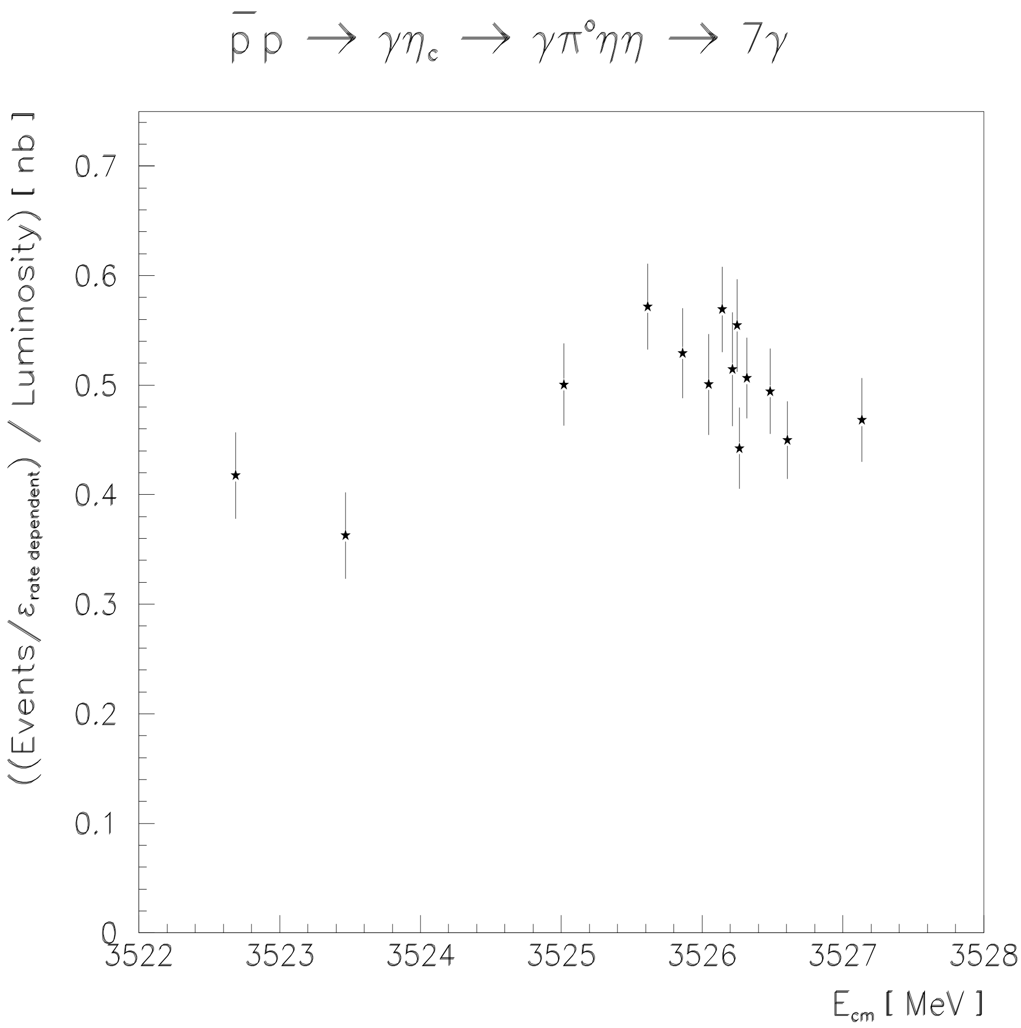


Figure 8.9: The results of the search for a resonance from $\bar{p}p \rightarrow \eta_c\gamma \rightarrow \pi^o\eta\eta\gamma$, a $7\gamma$ final state. The number of events is corrected on a run by run basis for the rate dependent efficiencies (binned by stack).

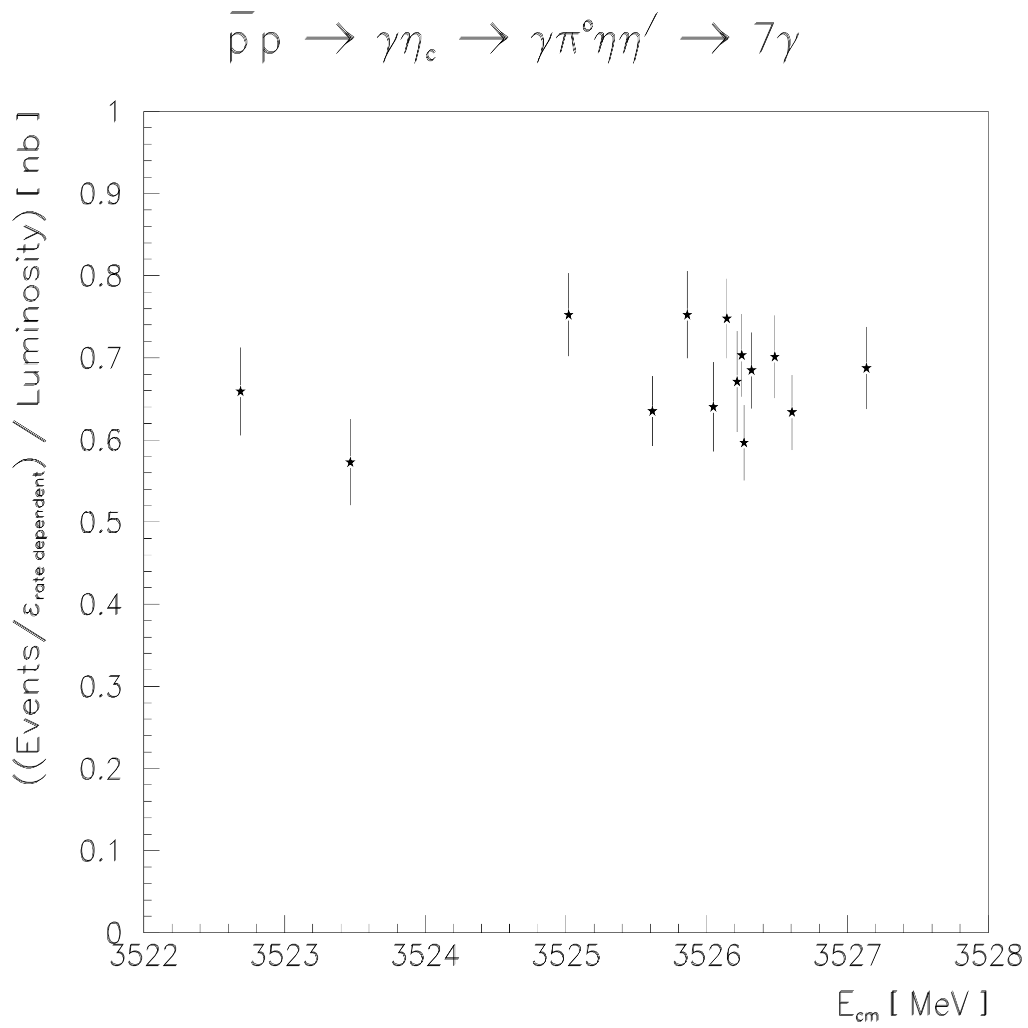


Figure 8.10: The results of the search for a resonance from $\bar{p}p \rightarrow \eta_c\gamma \rightarrow \pi^o\eta\eta'\gamma$, a $7\gamma$ final state. The number of events is corrected on a run by run basis for the rate dependent efficiencies (binned by stack).

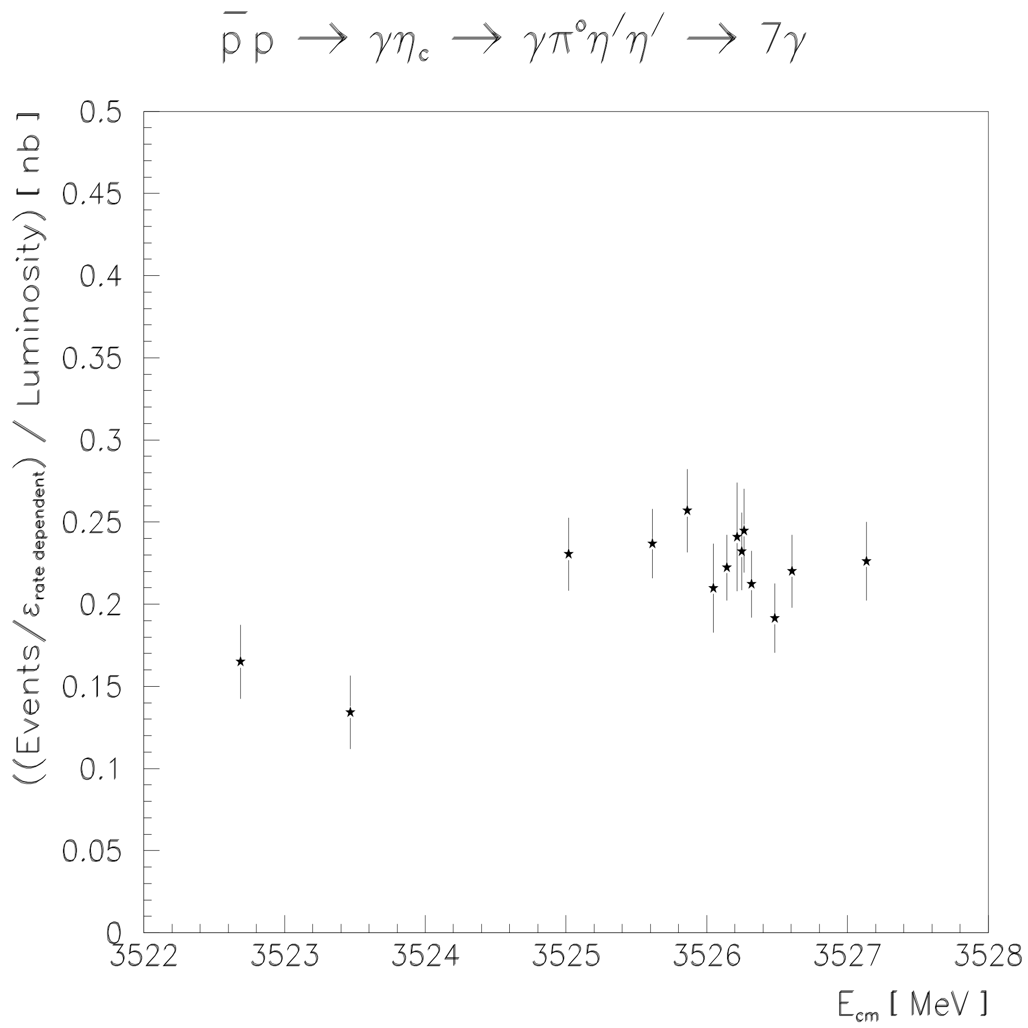


Figure 8.11: The results of the search for a resonance from $\bar{p}p \rightarrow \eta_c\gamma \rightarrow \pi^o\eta'\eta'\gamma$, a $7\gamma$ final state. The number of events is corrected on a run by run basis for the rate dependent efficiencies (binned by stack).

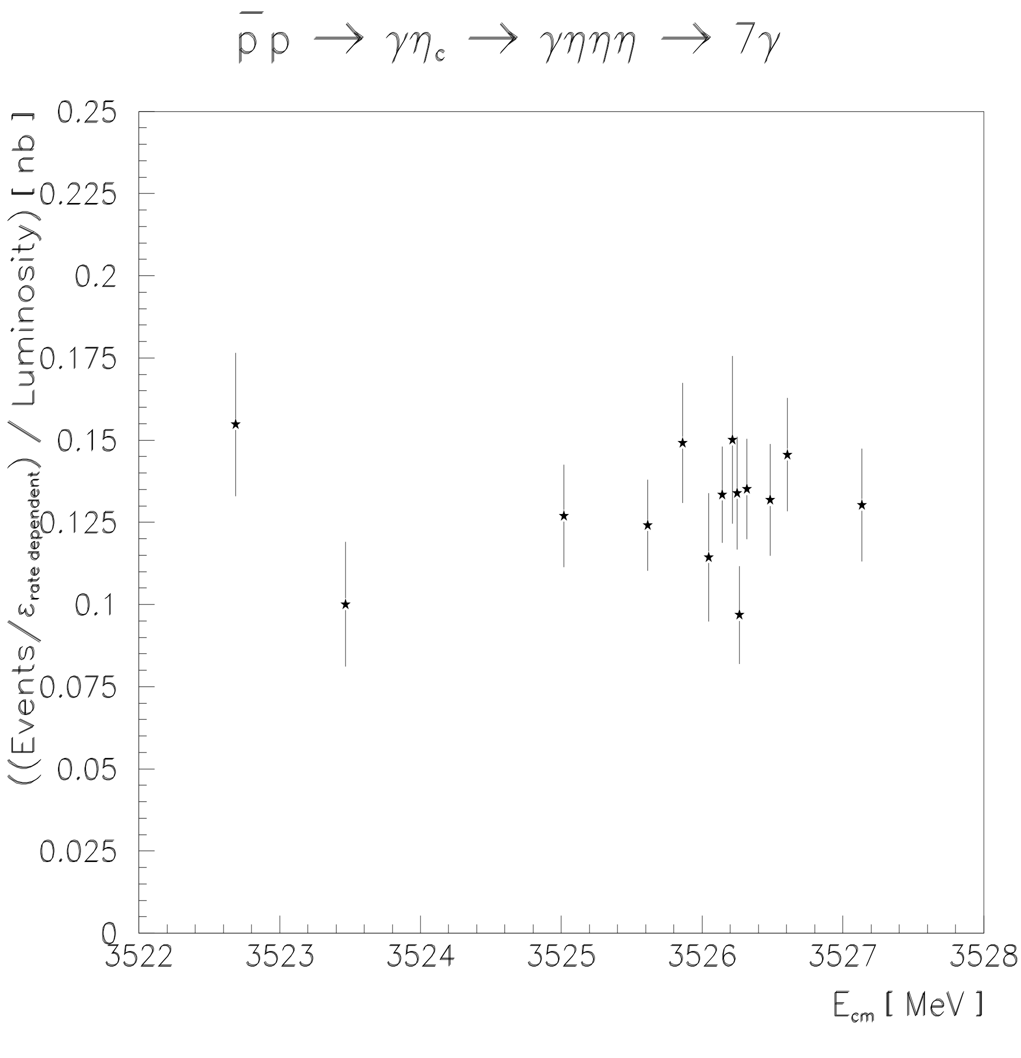


Figure 8.12: The results of the search for a resonance from $\bar{p}p \rightarrow \eta_c\gamma \rightarrow \eta\eta\eta\gamma$, a $7\gamma$ final state. The number of events is corrected on a run by run basis for the rate dependent efficiencies (binned by stack).

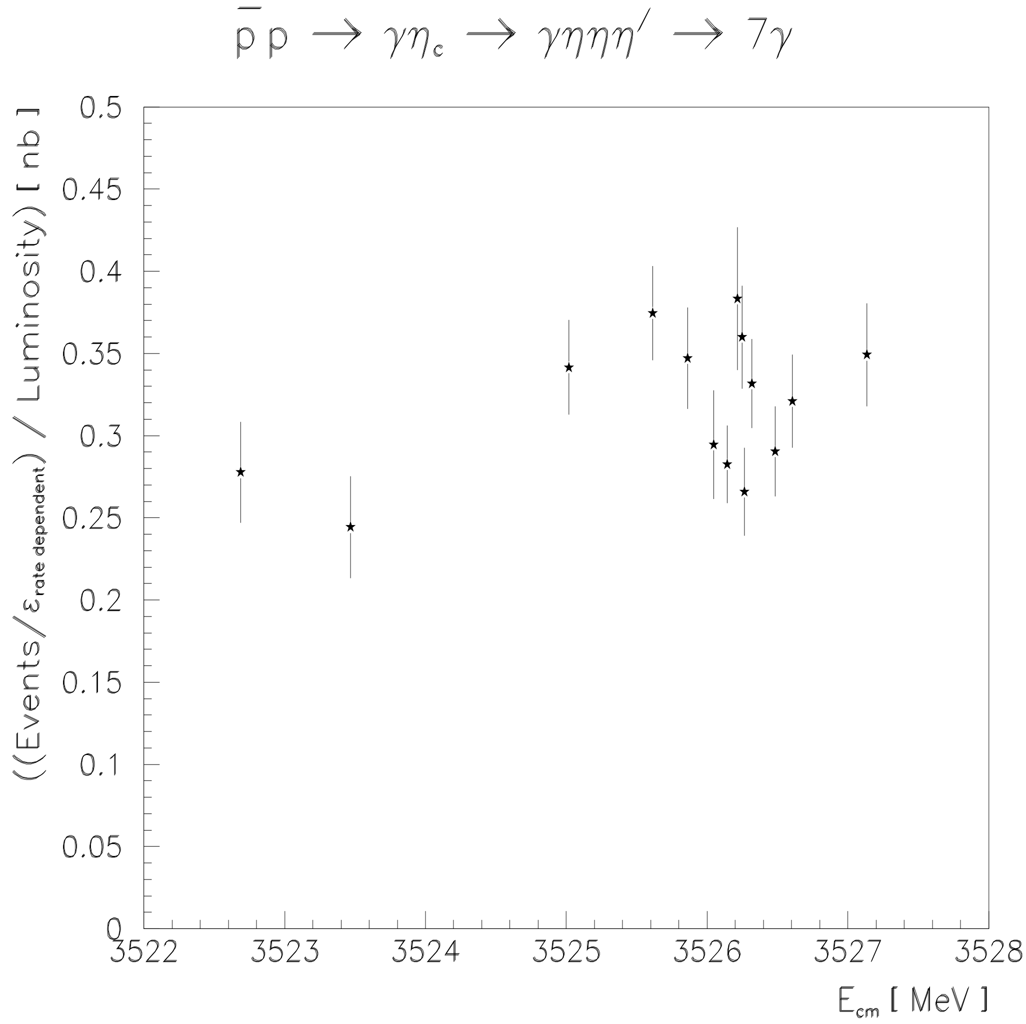


Figure 8.13: The results of the search for a resonance from $\bar{p}p \rightarrow \eta_c\gamma \rightarrow \eta\eta\eta'\gamma$, a $7\gamma$ final state. The number of events is corrected on a run by run basis for the rate dependent efficiencies (binned by stack).

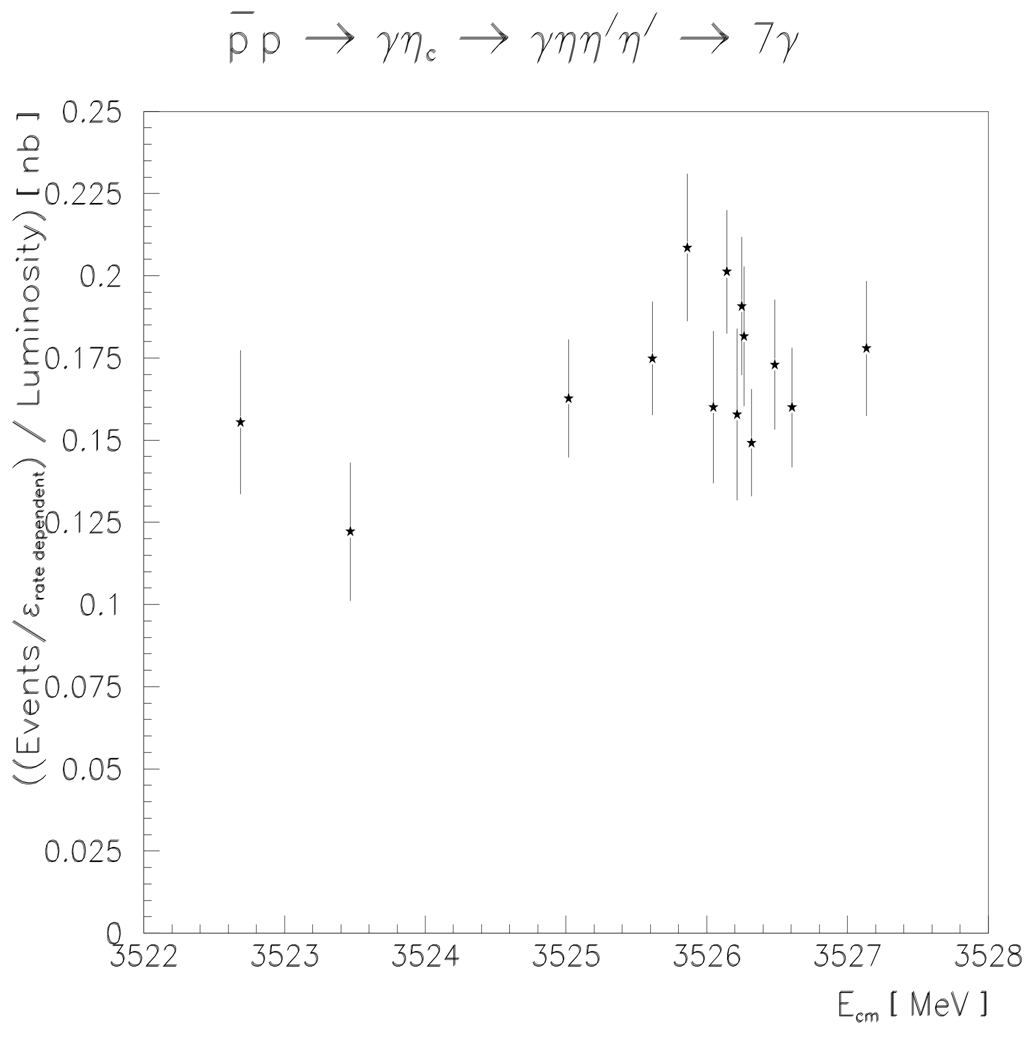


Figure 8.14: The results of the search for a resonance from $\bar{p}p \rightarrow \eta_c\gamma \rightarrow \eta\eta'\eta'\gamma$, a $7\gamma$ final state. The number of events is corrected on a run by run basis for the rate dependent efficiencies (binned by stack).

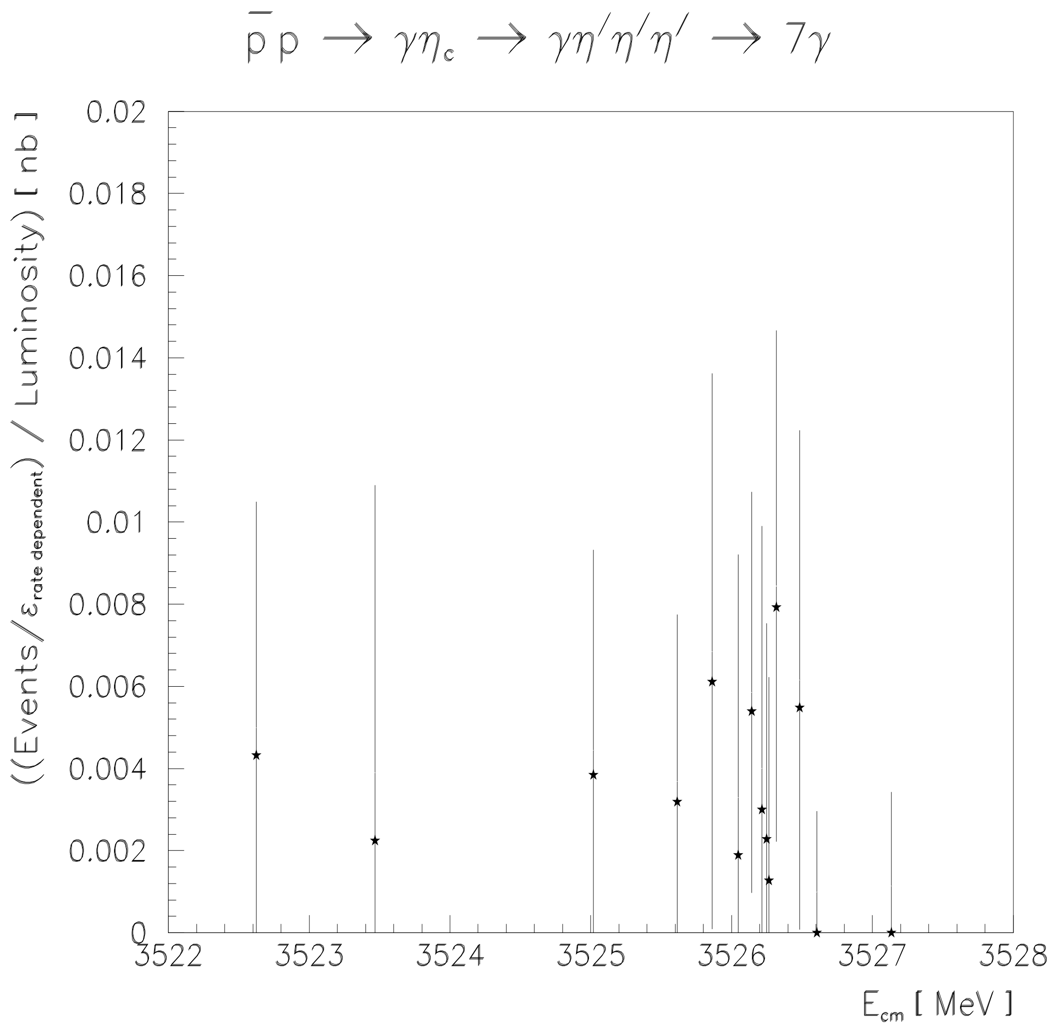


Figure 8.15: The results of the search for a resonance from $\bar{p}p \to \eta_c\gamma \to \eta'\eta'\eta'\gamma$, a $7\gamma$ final state. The number of events is corrected on a run by run basis for the rate dependent efficiencies (binned by stack).

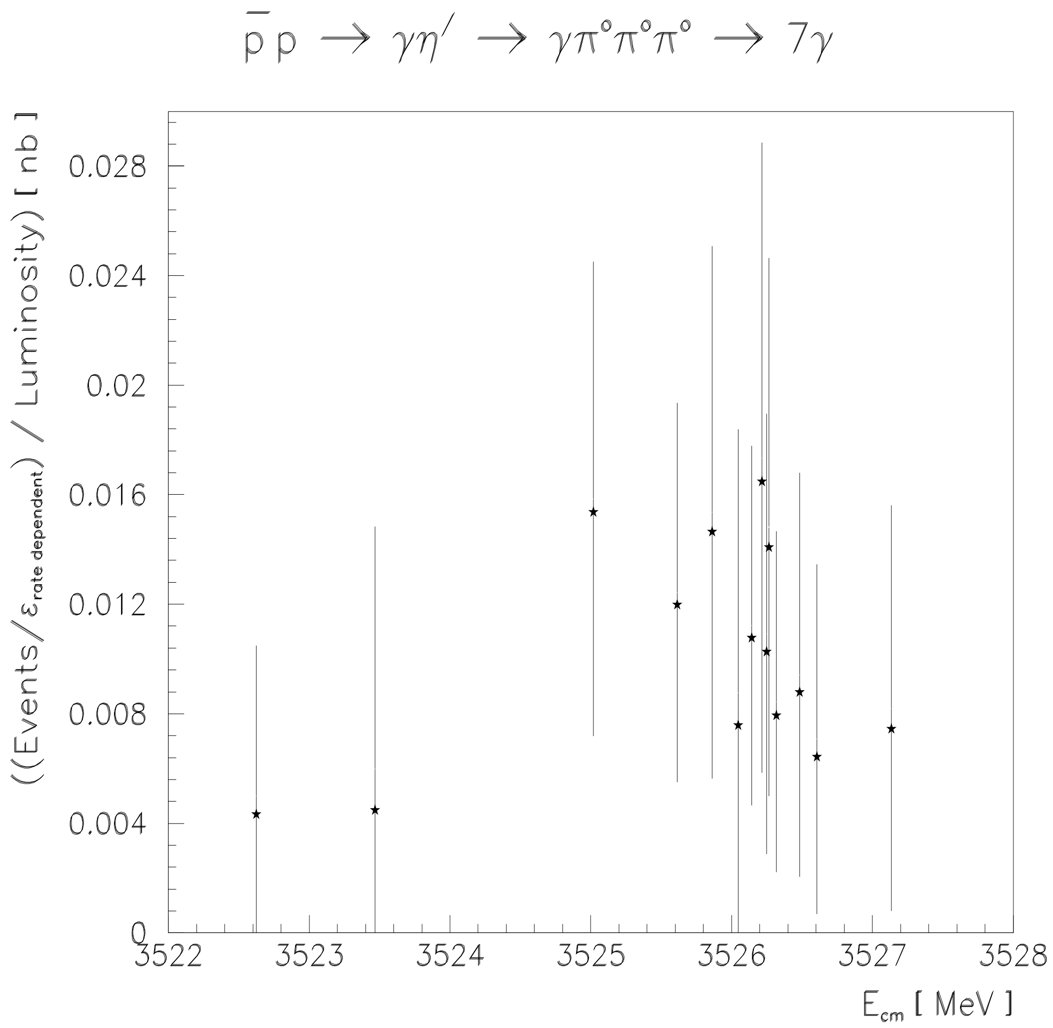


Figure 8.16: The results of the search for a resonance from $\bar{p}p \to \eta'\gamma \to \pi^o\pi^o\pi^o\gamma$, a $7\gamma$ final state. The number of events is corrected on a run by run basis for the rate dependent efficiencies (binned by stack).

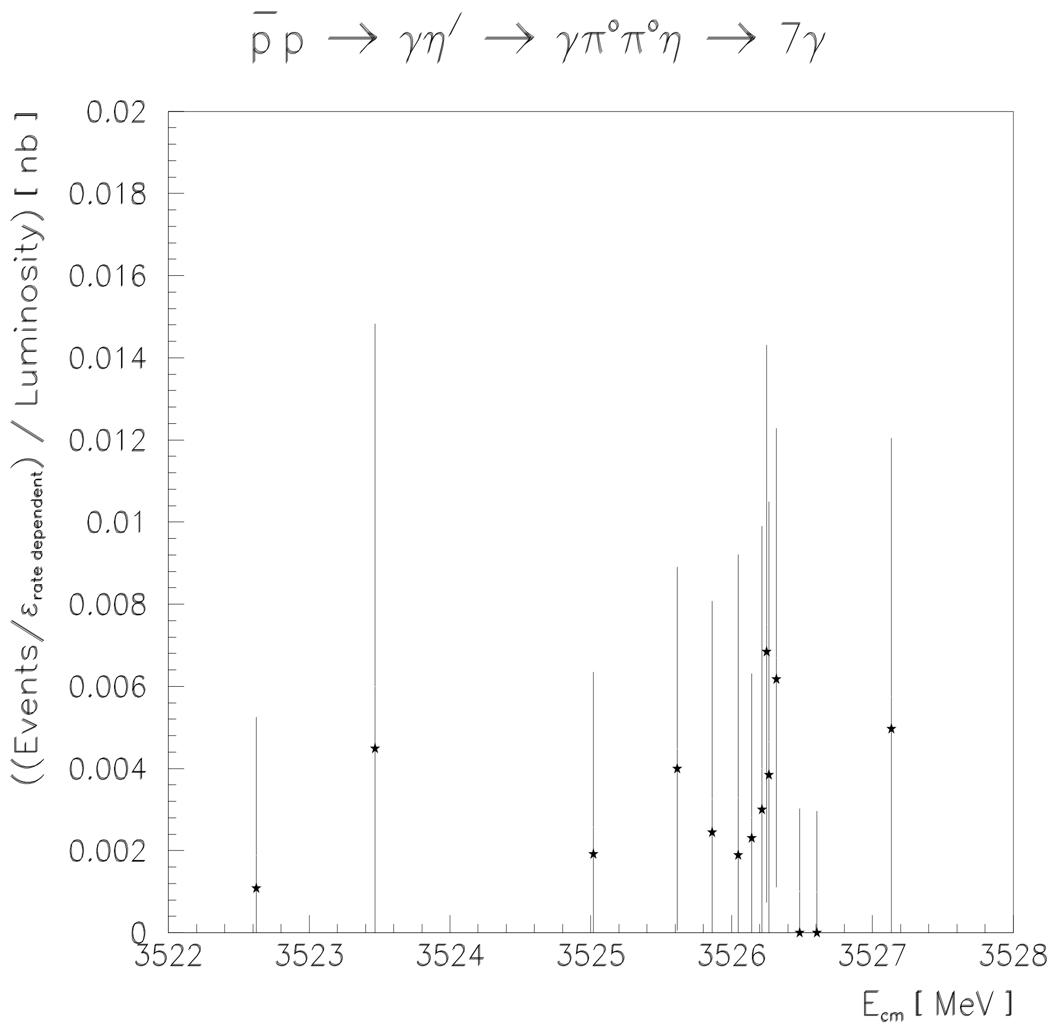


Figure 8.17: The results of the search for a resonance from $\bar{p}p \rightarrow \eta'\gamma \rightarrow \pi^o\pi^o\eta\gamma$, a $7\gamma$ final state. The number of events is corrected on a run by run basis for the rate dependent efficiencies (binned by stack).

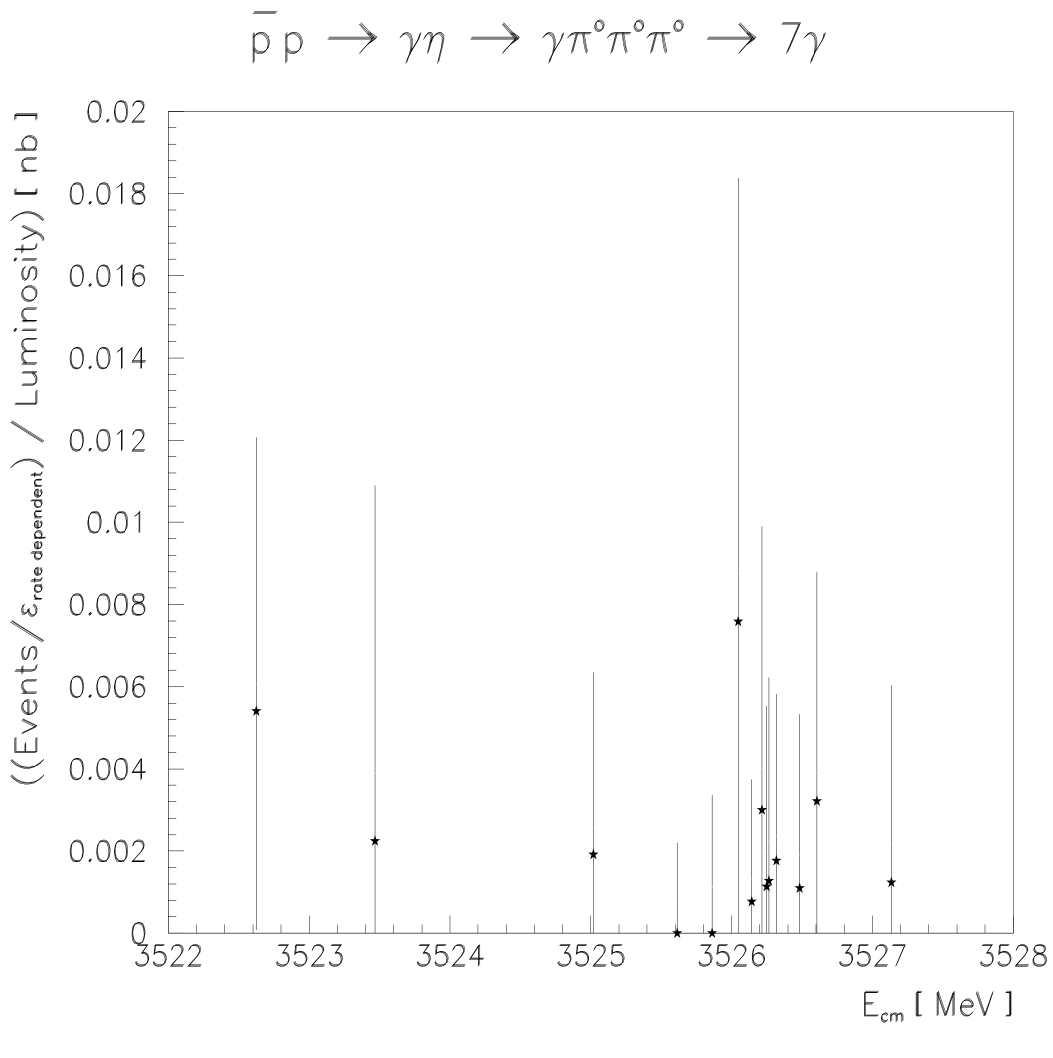


Figure 8.18: The results of the search for a resonance from $\bar{p}p \rightarrow \eta\gamma \rightarrow \pi^o\pi^o\pi^o\gamma$, a $7\gamma$ final state. The number of events is corrected on a run by run basis for the rate dependent efficiencies (binned by stack).

| $7\gamma$ State | Branching Ratio Product Upper Limit (90% $CL$) | | |
|---|---|---|---|
| $\gamma\eta_c \rightarrow \gamma\pi^o\pi^o\eta$ | $B(^1\mathrm{P}_1 \rightarrow \bar{p}p)B(^1\mathrm{P}_1 \rightarrow \gamma\eta_c)$ | $\leq$ | $1.1 \times 10^{-4}$ |
| $\gamma\eta_c \rightarrow \gamma\pi^o\pi^o\eta'$ | $B(^1\mathrm{P}_1 \rightarrow \bar{p}p)B(^1\mathrm{P}_1 \rightarrow \gamma\eta_c)$ | $\leq$ | $2.2 \times 10^{-3}$ |
| $\gamma\eta_c \rightarrow \gamma\pi^o\pi^o\pi^o$ | $B(^1\mathrm{P}_1 \rightarrow \bar{p}p)B(^1\mathrm{P}_1 \rightarrow \gamma\eta_c)B(\eta_c \rightarrow \pi^o\pi^o\pi^o)$ | $\leq$ | $1.6 \times 10^{-6}$ |
| $\gamma\eta_c \rightarrow \gamma\pi^o\eta\eta$ | $B(^1\mathrm{P}_1 \rightarrow \bar{p}p)B(^1\mathrm{P}_1 \rightarrow \gamma\eta_c)B(\eta_c \rightarrow \pi^o\eta\eta)$ | $\leq$ | $1.1 \times 10^{-5}$ |
| $\gamma\eta_c \rightarrow \gamma\pi^o\eta\eta'$ | $B(^1\mathrm{P}_1 \rightarrow \bar{p}p)B(^1\mathrm{P}_1 \rightarrow \gamma\eta_c)B(\eta_c \rightarrow \pi^o\eta\eta')$ | $\leq$ | $2.5 \times 10^{-4}$ |
| $\gamma\eta_c \rightarrow \gamma\pi^o\eta'\eta'$ | $B(^1\mathrm{P}_1 \rightarrow \bar{p}p)B(^1\mathrm{P}_1 \rightarrow \gamma\eta_c)B(\eta_c \rightarrow \pi^o\eta'\eta')$ | $\leq$ | $1.7 \times 10^{-3}$ |
| $\gamma\eta_c \rightarrow \gamma\eta\eta\eta$ | $B(^1\mathrm{P}_1 \rightarrow \bar{p}p)B(^1\mathrm{P}_1 \rightarrow \gamma\eta_c)B(\eta_c \rightarrow \eta\eta\eta)$ | $\leq$ | $7.8 \times 10^{-6}$ |
| $\gamma\eta_c \rightarrow \gamma\eta\eta\eta'$ | $B(^1\mathrm{P}_1 \rightarrow \bar{p}p)B(^1\mathrm{P}_1 \rightarrow \gamma\eta_c)B(\eta_c \rightarrow \eta\eta\eta')$ | $\leq$ | $1.7 \times 10^{-4}$ |
| $\gamma\eta_c \rightarrow \gamma\eta\eta'\eta'$ | $B(^1\mathrm{P}_1 \rightarrow \bar{p}p)B(^1\mathrm{P}_1 \rightarrow \gamma\eta_c)B(\eta_c \rightarrow \eta\eta'\eta')$ | $\leq$ | $3.9 \times 10^{-3}$ |
| $\gamma\eta_c \rightarrow \gamma\eta'\eta'\eta'$ | $B(^1\mathrm{P}_1 \rightarrow \bar{p}p)B(^1\mathrm{P}_1 \rightarrow \gamma\eta_c)B(\eta_c \rightarrow \eta'\eta'\eta')$ | $\leq$ | $5.5 \times 10^{-3}$ |
| $\gamma\eta' \rightarrow \gamma\pi^o\pi^o\pi^o$ | $B(^1\mathrm{P}_1 \rightarrow \bar{p}p)B(^1\mathrm{P}_1 \rightarrow \gamma\eta')$ | $\leq$ | $5.8 \times 10^{-5}$ |
| $\gamma\eta' \rightarrow \gamma\pi^o\pi^o\eta$ | $B(^1\mathrm{P}_1 \rightarrow \bar{p}p)B(^1\mathrm{P}_1 \rightarrow \gamma\eta')$ | $\leq$ | $5.6 \times 10^{-7}$ |
| $\gamma\eta \rightarrow \gamma\pi^o\pi^o\pi^o$ | $B(^1\mathrm{P}_1 \rightarrow \bar{p}p)B(^1\mathrm{P}_1 \rightarrow \gamma\eta)$ | $\leq$ | $7.7 \times 10^{-8}$ |

Table 8.4: The upper limits (90% $CL$) for the product of branching fractions from the $7\gamma$ channel analyses. The method is outlined in the text using the known branching fractions from reference [21].

divided by the integrated luminosity for the stack. Upper limits from the $7\gamma$ analysis can be placed upon the product of branching fractions in the same manner as has been done with the $3\gamma$ final state; the results are shown in table 8.4. Known branching fractions from reference [21] have been used.

## 8.5 Discussion

The $^1\mathrm{P}_1$ resonance has been detected through the decay to $J/\psi\pi^o$. The mass of the $^1\mathrm{P}_1$ is found to be

$$M_{h_c} = 3526.15 \pm 0.15 \pm 0.19 \ \mathrm{MeV/c}^2, \tag{8.15}$$

where the first error is the statistical error as determined from the fit and the second error is the systematic error from the uncertainty of the beam energy calibration.

This implies the hyperfine mass splitting (equation 1.41) is

$$\Delta_{HF} = 0.88 \pm 0.47 \text{ MeV}; \tag{8.16}$$

therefore, $M_{h_c} > M_{\chi_{cog}}$. An upper limit (90% $CL$) of the resonance width is set at

$$\Gamma_{h_c} \leq 1.1 \text{ MeV}. \tag{8.17}$$

A determination of the width is not possible in these data due to the low statistics and large width of the beam energy distribution. Assuming 1.0 MeV $\geq \Gamma_{h_c} \geq$ 0.5 MeV, the product of the production and decay branching ratios of the $^1\mathrm{P}_1$ is

$$(1.2 \pm 0.4) \times 10^{-7} \leq B(^1\mathrm{P}_1 \to \bar{p}p)B(^1\mathrm{P}_1 \to J/\psi\pi^o) \leq (1.7 \pm 0.5) \times 10^{-7}. \tag{8.18}$$

If the largest predicted partial width for the $J/\psi\pi^o$ decay from table 1.4, 2 keV, and a 750 keV total width is assumed, then the production branching fraction is $5.5 \times 10^{-5}$ which is close to the corresponding value for the $\chi_1$.

E760's measurement of the $^1\mathrm{P}_1$ conflicts with the R704 interpretation of its five $J/\psi + X$ events as a resonance. When R704's energy scale is adjusted by using both experiments' measurements of the $\chi_1$ and $\chi_2$ masses, the five events are centered at $3524.60 \pm 0.85$ MeV/c$^2$, less than $M_{\chi_{cog}}$, or $\Delta_{HF}$ is $-0.67 \pm 1.08$. This is different from (1.55 MeV lower), but not incompatible with, the E760 result (equation 8.16). The five events also imply an order of magnitude larger product of branching ratios than found above; if R704's resonance interpretation is true, E760 should have seen an excess of several hundred events. E760 has not seen such a large signal. One of the five events can be attributed to the same background as seen by E760, the $J/\psi\pi^o$

continuum and $J/\psi\gamma$, and the remaining four events may be misidentified $\bar{p}p \to \pi^o\pi^o$ (where the $\pi^o$'s undergo Dalitz decay and/or gamma rays convert in the beam pipe). When the E760 charged data set is subject to the analysis cuts applied by R704 and corrections are made for the different acceptances and integrated luminosities, four such events result. Hence, the five $J/\psi + X$ events that R704 observed near the expected $^1\mathrm{P}_1$ mass are most likely background events.

An upper limit for the $^1\mathrm{P}_1$ to decay to $J/\psi\pi\pi$ can be determined from the two upper limits for $J/\psi\pi^o\pi^o$ and $J/\psi\pi^+\pi^-$ (equations 8.8 and 8.9). The combined limit[4] assumes one third of the $J/\psi\pi\pi$ decays will be $J/\psi\pi^o\pi^o$ decays. The upper limit (90% $CL$) for product of branching ratios is

$$B(^1\mathrm{P}_1 \to \bar{p}p) \times B(^1\mathrm{P}_1 \to J/\psi\pi\pi) \leq 3.2 \times 10^{-8}. \tag{8.19}$$

Using this result and the product of branching ratios for a 750 keV resonance width from the $J/\psi\pi^o$ analysis (see table 8.2), an upper limit (90% $CL$) can be set

$$\frac{B(^1\mathrm{P}_1 \to J/\psi\pi\pi)}{B(^1\mathrm{P}_1 \to J/\psi\pi^o)} \leq 0.21. \tag{8.20}$$

Predicted values for this ratio (see tables 1.3 and 1.4) are greater than 2; the experimental limit is not compatible with any of these predictions. However, Voloshin [83] predicts that hadronic transitions from an excited triplet S state to the singlet P state in the bottomonium system will favor $\pi^o$ over $\pi\pi$ (by an order of magnitude). If the same prediction applies to the hadronic transitions in charmonium from the $^1\mathrm{P}_1$ to the $J/\psi$, then this prediction is in agreement with E760's experimental result.

[4] Independent upper limit measurements $\Gamma_i$ for the same mode result in the combined upper limit $\frac{1}{\Gamma} \geq \sum \frac{1}{\Gamma_i}$.

The upper limit (90% $CL$) for the product of branching ratios of the expected dominant decay channel and the production channel is

$$B(^1\mathrm{P}_1 \rightarrow \bar{p}p) \times B(^1\mathrm{P}_1 \rightarrow \gamma\eta_c) \leq 2.6 \times 10^{-5}; \tag{8.21}$$

this limit is the combined upper limits for the $3\gamma$ final state (equation 8.13) and two $7\gamma$ final states (the first two entries in table 8.4). If the branching fraction for production found above, using the assumptions of 750 keV total width and 2 keV $J/\psi\pi^o$ partial width of the $^1\mathrm{P}_1$, then $B(^1\mathrm{P}_1 \rightarrow \gamma\eta_c) \leq 0.47$; however, this uses a partial width from a method that predicts a ratio for the hadronic transitions which contradicts E760's result, equation 8.20. Of course, if $B(^1\mathrm{P}_1 \rightarrow \bar{p}p)$ is smaller then $B(^1\mathrm{P}_1 \rightarrow \gamma\eta_c)$ is larger and $\gamma\eta_c$ can be the dominating partial width.

Other upper limits for the product of branching ratios for $7\gamma$ final states involving unobserved $\eta_c$ decay modes are in table 8.4. Also included in the table are product of branching fractions for radiative decays to $\eta'$ and $\eta$; the upper limits (90% $CL$) are

$$B(^1\mathrm{P}_1 \rightarrow \bar{p}p) \times B(^1\mathrm{P}_1 \rightarrow \gamma\eta') \leq 5.5 \times 10^{-7}, \tag{8.22}$$

where two limits are combined, and

$$B(^1\mathrm{P}_1 \rightarrow \bar{p}p) \times B(^1\mathrm{P}_1 \rightarrow \gamma\eta) \leq 7.7 \times 10^{-8}. \tag{8.23}$$

## 8.6 Conclusion

A resonance has been found in $\bar{p}p$ annihilations near the spin weighted center of gravity of the triplet P wave charmonium states; the resonance is identified as the singlet P wave state, ${}^1\mathrm{P}_1$ or $h_c$. E760 is the first experiment to observe the singlet P state in charmonium. The ${}^1\mathrm{P}_1$ has only been observed in one decay channel ($J/\psi\pi^o$) with small statistics; however, the probability that the data is a fluctuation from a flat background is small ($\approx 10^{-3}$). Searches for a less than 1 MeV wide resonance in other decay channels ($J/\psi\pi\pi$, $\gamma\eta_c$, $\gamma\eta'$, and $\gamma\eta$) give null results and upper limits to the product of branching ratios have been set. Future work by the E760 collaboration will attempt to confirm this result and, hopefully, will observe the ${}^1\mathrm{P}_1$ in more than the one decay channel.